Textures and Microstructures, Vol. 34, pp. 75–90
Reprints available directly from the publisher
Photocopying permitted by license only

SIMULATION OF TEXTURE FORMATION IN A ZrO_2 FILM GROWN ON Zr–2.5%Nb

H. LI*, M. GLAVICIC and J.A. SZPUNAR

Department of Metallurgical Engineering, McGill University, Montreal, Canada, H3A 2B2

(Received 8 October 1999)

A computer model is developed which is capable of simulating the texture and microstructure of the oxide grown on a Zr substrate. In this computer model, the effects of both substrate texture and microstructure in the formation of oxide texture and microstructure are taken into account. The substrate and oxide are represented with digitized unit cells. Each unit cell has an orientation characterized by three Euler angles. In the nucleation and re-nucleation stage, the orientation of each oxide cell is determined by substrate orientation and microstructure. In the oxide grain growth stage, the orientation of each oxide cell is determined by minimizing the stress at the oxide/metal interface. In this paper, the model is applied to the simulation of the texture formation of the ZrO_2 grown on a Zr–2.5%Nb substrate. Three substrates with completely different orientations and microstructures are used in the study. Good agreement between the simulated and the experimental results is obtained.

Keywords: Simulation; Oxidation; ZrO_2; Texture; Microstructure; Zr–2.5%Nb

INTRODUCTION

Zr–2.5%Nb alloy pressure tubes are used in the core of CANDU nuclear power reactors. The interior surface of the tube is in contact with the heavy water (D_2O) coolant that contains dissolved hydrogen, while the exterior surface is in contact with a dry N_2 or CO_2 annulus gas containing a small amount of oxygen and hydrogen. During the

* Corresponding author.

operation of the reactor, oxidation takes place on both the interior and exterior surfaces. The oxide film formed on the pressure tube surface is a good protective barrier against further oxidation and hydrogen ingress, both of which have a deleterious influence on the mechanical properties of the Zr–2.5%Nb alloy. The oxidation process and hydrogen ingress are both inward diffusion processes. One of the major factors that affects the diffusion process is the oxide texture, which determines the grain boundary character distribution (GBCD). Understanding of the oxide texture formation is therefore critical to the understanding of how and to what extent the oxide film can protect the alloy from further oxidation and hydrogen ingress.

Earlier studies on the formation of oxide texture have mainly focused on the epitaxial orientation relationship between the ZrO_2 and α-Zr substrate. Ploc (1983) suggested an epitaxial orientation relationship of $[001]_m||[11\bar{2}0]_\alpha$ and $(100)_m||(0001)_\alpha$ between the monoclinic oxide (m) and the hexagonal substrate (α) based on the observation of TEM pictures. Lin *et al.* (1994) showed that the orientation relationship was $[100]_m||[4\bar{5}10]_\alpha$ and $(010)_m||(0001)_\alpha$. Although these orientation relationships can explain approximately the major orientations of the oxide formed on the radial face of the pressure tube, they cannot explain the texture of oxide formed on other substrates. This indicates that the microstructural mechanisms of the texture formation of the oxide on Zr–2.5%Nb is more complicated. Recently, a ZrO_2 texture formation mechanism was proposed by Li *et al.* (1999). With this mechanism, both the major and minor orientations of the oxide formed on different substrates can be explained. In this paper, a computer model based on the previously proposed oxidation mechanism of Zr (Li *et al.*, 1999) is developed. The model is applied to the simulation of the texture formation of the oxide grown on the radial, tangential and longitudinal faces of the pressure tube.

A CELLULAR MODEL OF ZrO_2 TEXTURE AND MICROSTRUCTURE FORMATION

A Brief Description of the ZrO_2 Oxidation Process

When a metal with a clean surface is exposed to oxygen, the adsorption of oxygen atoms takes place first. The adsorbed oxygen atoms diffuse

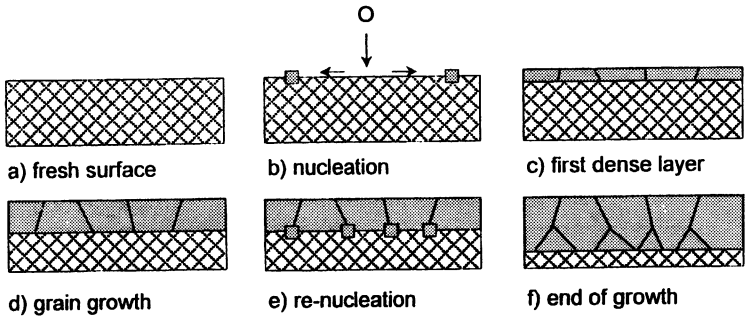

FIGURE 1 A simplified oxidation process.

on the metal surface (Kofstad, 1988). Eventually each will find a preferable nucleation site and becomes an oxide nucleus, or it will meet an existing oxide nucleus and join it by reacting with the metal atom as shown schematically in Fig. 1(b). After the nucleus grows laterally and forms a continuous layer, the oxygen and metal are separated by this layer of oxide (Fig. 1(c)). Further oxide growth will be controlled by inward oxygen diffusion though the previously developed oxide layer (Beie *et al.*, 1994). The oxide film grows uniformly towards the metal/oxide interface. During growth, some oxide grains grow faster laterally than their neighbors and become bigger (Fig. 1(d)). This causes the formation of the oxide texture and microstructure. Moreover, during the oxide growth stage, re-nucleation may take place somewhere and a new oxide grain may be generated (Fig. 1(e)). From the simplified oxidation process, it can be seen that the oxidation process consists of oxide nucleation, grain growth and re-nucleation. The simulation of oxidation is to realize the oxide nucleation, grain growth and re-nucleation processes in the computer.

A Cellular Model of Texture and Microstructure Formation

The whole simulation consists of two modules (Fig. 2): a simulation module and a plug-in module. The simulation module basically follows the simplified oxidation process described above. The plug-in module contains the oxidation parameters of ZrO_2 which controls the oxide nucleation, grain growth and re-nucleation processes.

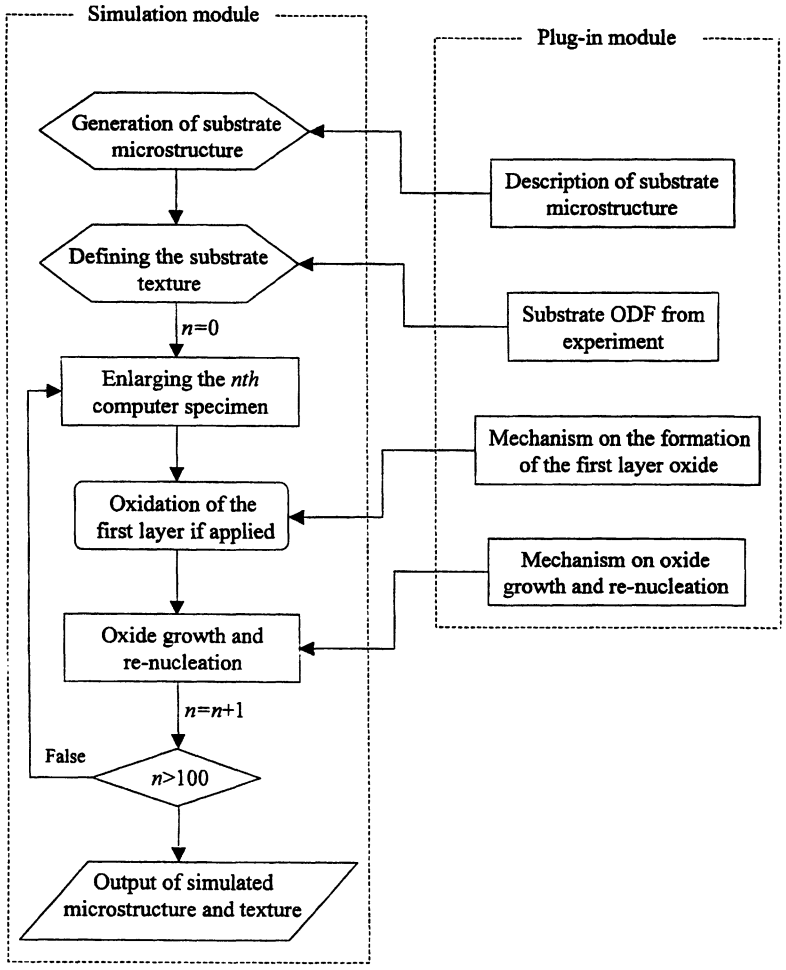

FIGURE 2 Flow chart of the simulation procedure.

The Simulation Module

Before introducing the model, it is necessary to describe how to represent the two-dimensional metal substrate and oxide structures. As can be seen in Fig. 3, both the substrate metal and oxide are represented by number of grains. Each grain is digitized into a number of cells. The cell is defined as a small area of oxide or metal in a square lattice. Each cell

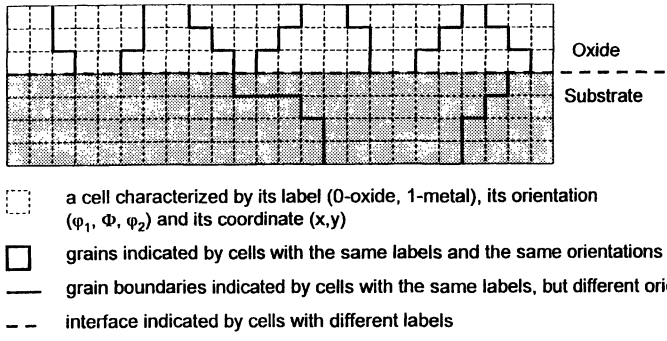

FIGURE 3 Cellular representations of oxide and substrate microstructures.

is distinguished by three properties, a label indicating the type of the cell (representing metal or oxide), a pair of integers representing the position of the cell and three integers representing the cell's orientation in three Euler angles ($\varphi_1, \Phi, \varphi_2$) where the three Euler angles are in a grid of 5° intervals. The cells with same labels and orientations compose a grain (metal or oxide grain). The cells with the same labels and different orientations compose a grain boundary. The cells with different labels compose a metal/oxide interface.

In step 1, a two-dimensional substrate microstructure containing Voronoi grains is generated using the Monte-Carlo method. The Voronoi grain is defined as that where all the cells within this grain are closer to the center of this grain than that of others. The centers of the n grains are randomly selected within the two-dimensional space $X \times Y$. A cell is taken to calculate the distance between this cell and each center $(C_1, C_2, \ldots, C_n)$. When the distance between the center C_m $(1 \leq m \leq n)$ and the cell is at a minimum among all the values obtained, the cell is marked with m. At this stage of the simulation, the label of the cell (first property of the cell) ranges from 1 to n, the position of the cell has been defined but the orientation of the cell is not defined. The dimension of the microstructure depends on the number of grains and the average number of cells in one grain. The number of grains determines how well the generated microstructure can represent the substrate ODF (Orientation Distribution Function) which is dependent on the crystal symmetry and sharpness of the texture. The number of 5000 grains has been proven to be more than enough for the given Zr substrate with a hexagonal crystal system. The average number of cells in one grain is

not really important since it will not affect the number of grain neighbors significantly for the microstructure generated with this method. The average number of grain neighbors is always close to 6 unless the number of cells in one grain is close to 1, which gives 4 neighbors for each grain. Clearly, the more cells used in one grain, the better the microstructure looks. Based on the above analysis, a dimension of 5000×100 is used for the generated substrate microstructure which is able to hold a maximum of 5000 grains with an average grain size of 100 cells. This microstructure has a longer width ($X = 5000$) and a shorter height ($Y = 100$). This is due to the fact that the oxide is formed as a thin film. This part of the computer code reads the description of the substrate microstrtucture from the plug-in module. It allows one to specify elongation along a certain direction (X or Y) and defects such as those of secondary phase. The computer generated microstructure is called a 'computer specimen' in the following section.

Step 2 in the simulation module is to distribute the experimental texture to the generated microstructure. Texture information from experiments are normally pole figures from which the ODF can be derived. The ODF is defined as the intensities of an orientation g as a function of orientation g where orientation g is represented by three Euler angles, $g \equiv (\varphi_1, \Phi, \varphi_2)$. Since the Euler angular space is not linear along Φ, the intensity of a particular orientation is not equal to its volume fraction which is used to define the texture of the computer specimen. Therefore, the volume fraction of the orientation g has to be calculated from ODF as

$$\frac{dV}{V} = f(g)\, dg, \tag{1}$$

where V is the normalized total volume of the specimen, $f(g)$ represents the ODF and the dg is the orientation volume (Bunge, 1982)

$$dg \equiv d(\varphi_1, \Phi, \varphi_2) = 1/8\pi^2 \sin \Phi\, d\Phi\, d\varphi_1\, d\varphi_2, \tag{2}$$

where $1/8\pi^2$ is the normalization factor to ensure that the summation of all orientations is 1 when Eq. (2) is integrated in the range of $0 \leq \varphi_1 \leq 2\pi$, $0 \leq \Phi \leq \pi$ and $0 \leq \varphi_2 \leq 2\pi$. In practice, the three Euler angles are used in degrees and the ODF is calculated in the grid of 5° intervals in $\varphi_1, \Phi, \varphi_2$. A particular orientation (fi_1, fi, fi_2) represents an

orientation volume in the range of $(\mathrm{fi}_1 - 2.5) \leq \varphi_1 \leq (\mathrm{fi}_1 + 2.5)$, $(\mathrm{fi} - 2.5) \leq \Phi \leq (\mathrm{fi} + 2.5)$, and $(\mathrm{fi}_2 - 2.5) \leq \varphi_2 \leq (\mathrm{fi}_2 + 2.5)$. Therefore, by substituting the Eq. (2) into (1) and integrating the Eq. (1), the volume fraction of an orientation of $(\mathrm{fi}_1, \mathrm{fi}, \mathrm{fi}_2)$ can be calculated from the ODF as

$$\Delta V = \frac{1}{8 \times 36 \times 36} f(g)(\cos(\mathrm{fi} - 2.5) - \cos(\mathrm{fi} + 2.5))$$

$$\propto f(g)(\cos(\mathrm{fi} - 2.5) - \cos(\mathrm{fi} + 2.5)). \tag{3}$$

In the simulation, Eq. (3) is used to calculate the volume fraction of orientation $(\mathrm{fi}_1, \mathrm{fi}, \mathrm{fi}_2)$ and then distribute it randomly to the computer specimen. The principle in the distribution procedure is to keep the number of grains with an orientation of $(\mathrm{fi}_1, \mathrm{fi}, \mathrm{fi}_2)$ proportional to its volume fraction. This is based on the assumption that all grains in the computer specimen have approximately the same size.

After the distribution of the ODF to the computer specimen, all three properties of the cell have been defined. The label of cells are set to 1, which means the whole computer specimen is not oxidized at this stage of the simulation.

In step 3, one percent of the computer specimen, with a dimension of 500×10, is cut from the defined computer specimen. This piece of computer specimen is then enlarged and sent through the following simulation procedure. The reason for this is given below. In a real situation, the grain size of the substrate metal is much larger than that of the oxide. Hundreds of oxide grains may be formed within one substrate grain. The large substrate grain in the computer specimen are preferred in order to make sure that different oxide nuclei and oxide grains can be formed in one substrate grain. Although we do not know how many cells within one substrate grain are enough, we want the substrate grain to be able to hold as many oxide grains as possible. In the computer specimen generated in step 1, the average number of cells in one substrate grain is 100. Obviously this is not enough to hold hundreds of oxide grains. Therefore, in this part of the program the computer specimen is enlarged by a factor of 100. Thus, every 1% of the computer specimen has a dimension 5000×100. This dimension is determined based on the consideration of computer memory. The microstructure

with a dimension of 5000 × 100 needs approximately 6 MB of computer memory to store it. This is a good range for a PC with a memory from 16 to 32 MB.

In stage 4, 1% of the computer specimen from step 3 is taken to simulate the oxidation process. Nucleation takes place if this piece of computer specimen contains the metal surface. A random number between 1 and 5000 is generated to represent the position of oxygen atom which is adsorbed on the metal surface. This oxygen atom is then allowed to diffuse on the surface within n steps where the number n is arbitrarily defined. In this two-dimensional model, the direction of the surface diffusion is selected between left and right by a random number. During the diffusion process, the oxygen atom may reach a suitable nucleation location or meet an existing oxide grain. If the former case takes place first, the cell at that position becomes an oxide nucleus, its label is set to 0 and its orientation is assigned. Both the nucleation position and the oxide orientation are determined according to the oxidation mechanism specified in the plug-in module, which is explained later. If the latter case takes place first, the cell at that position becomes an adoxide and its orientation is inherited from that of the existing oxide grain. If neither of them takes place, then de-adsorption is assumed to occur and the oxygen atom disappears from the simulation. This process continues until a complete layer of oxide is formed.

In stage 5, the oxide formed in step 4 is allowed to grow. This growth process is realized in the computer by changing the substrate cells to oxide cells and assigning the oxide cells new orientations. The oxide film is assumed to grow layer by layer. As the oxide grows, the labels of the cells in that layer are changed from 1 to 0 which represents the oxide. Their orientations are the same as that of the oxide cells in the previous layer if the positions of the cells are not re-nucleation positions. Otherwise, re-nucleation takes place and new orientations are assigned to the cells. which is determined by the oxidation mechanism specified in the plug-in model. After all labels of the cells in this layer are changed to 0 and the cell orientations have been assigned, each cell is given n trials to change its orientation. The orientation of the cell can only be either that of itself or that of its neighbors, which means that no re-nucleation takes place in this orientation changing process.

The criterion for this process

$$P = \begin{cases} 1 & Q_{new} \leq Q_{old} \\ \exp(-\beta(Q_{new} - Q_{old})/Q_{old}) & Q_{new} > Q_{old} \end{cases}, \quad (4)$$

where P is the probability of success, β is a factor defined arbitrarily to control the difficulty of the up-hill process and Q represents the effective 'base area' of an orientation which is explained in the plug-in module. Steps 4 and 5 are repeated until the entire computer specimen is simulated.

In step 6, the qualitative oxide texture and microstructure information from the simulation are generated. The number of oxide cells, as a function of the three Euler angles, are counted. This function after normalization is the simulated qualitative ODF. The simulated ODF can be used to generate pole figures. The simulated oxide microstructure can be obtained by drawing a boundary line between the cells with different orientations and the same labels.

The Plug-In Module

In the plug-in module, the substrate microstructure, texture and the oxidation mechanism are specified. The substrate Zr–2.5% alloy is known to contain two phases, α-Zr (Zr–1%Nb) and β-Zr (Zr–20%Nb). The α-Zr grain has a grain shape with an aspect ratio of 1 : 5 : 50 along the radial, tangential and longitudinal directions and is surrounded by β-Zr with a volume fraction of 8%. According to this information, the substrate microstructure of the computer specimen can be defined. The orientations of the substrate grains in the computer specimen are determined by the ODF calculated from experimental pole figures. The nucleation positions are the α-Zr grain boundary regions and β-Zr regions according to the previously proposed oxidation mechanism (Li *et al.*, 1999). The orientations of the oxide nuclei are determined by lattice matching between the substrate and oxide orientations. The oxide orientations with a small 'base area' are considered favorable in the grain growth stage in order to reduce the biaxial stress at the interface, which is generated by the area difference occupied by the oxide and metal (Li *et al.*, 1999). The term 'base area' of an orientation $(hkl)[uvw]$ is defined as the projection area of the

(*hkl*)[*uvw*] unit cell when this unit cell is projected to the (*hkl*) crystallographic plane. Since each oxide orientation experiences a different amount of deformation under the same stress, the amount of deformation is deduced from the 'base area' and it is called the effective 'base area'. In the simulation, the effective 'base area' is the factor which controls oxide grain growth.

SIMULATION RESULTS AND DISCUSSION

Three sets of simulation have been performed on samples cut from radial (RD), tangential (TD) and longitudinal (LD) faces of the pressure tube to emphasize the difference in substrate orientations. The ideal orientations for the three samples are shown in Table I.

For the ideal orientation of sample RD, crystallographic plane $(1\bar{1}00)$ is parallel to the sample surface. The $[1\bar{1}00]$ and $[000\bar{1}]$ crystallographic directions lie in the sample surface and are perpendicular to each other. Due to lattice matching between the oxide and substrate the simulation shows that the following oxide orientation with its *a*, *b* or *c* axes parallel to $[1\bar{1}00]$ or $[000\bar{1}]$ are favorable in the nucleation stage:

$\{0nm\}\langle 100\rangle$ (*a*, *b*, *c* axes of monoclinic oxide parallel to the substrate $[1\bar{1}00]$)

$\{0nm\}\langle 0\bar{m}n\rangle$ (*a*, *b*, axes of monoclinic oxide parallel to the substrate $[000\bar{1}]$)

where *n* and *m* are arbitrary Miller indices. Among the oxide orientations in this group, the $\{001\}\langle 100\rangle$ orientations that have two out of three *a*, *b*, *c* axes parallel to the $[1\bar{1}00]$ and $[000\bar{1}]$ directions on the substrate surface, are more favorable than the orientations that have one out of three axes parallel to the $[1\bar{1}00]$ and $[000\bar{1}]$. As a result, the $\{001\}\langle 100\rangle$ orientation should dominate in the nucleation stage. This

TABLE I The ideal substrate orientations of three samples

Samples	*Orientations*
RD	$(11\bar{2}0)[1\bar{1}00]$
TD	$(0001)[1\bar{1}00]$
LD	$(1\bar{1}00)[0001]$

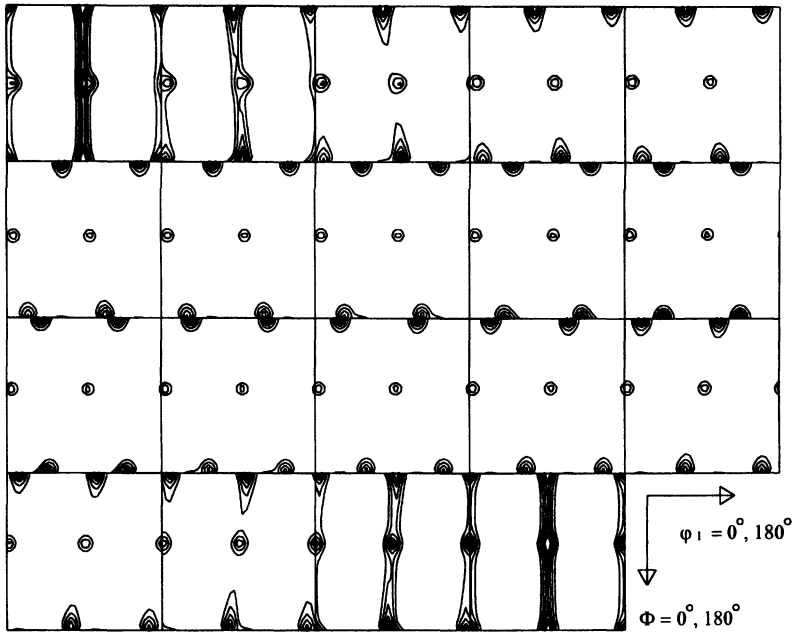

FIGURE 4 The simulated ODF of oxide formed on the ideal orientation of sample RD at the nucleation stage.

has been confirmed by experimental results (Li *et al.*, 1999). The simulated oxide ODF in the nucleation stage is shown in Fig. 4. The peaks on the ODF correspond to $\{001\}\langle 100\rangle$ orientations. The ODF is drawn within the Euler angular range of $0 \leq \varphi_1 \leq \pi$, $0 \leq \Phi \leq \pi$, $0 \leq \varphi_2 \leq \pi/2$ since the oxide has a 2-fold crystal symmetry and 4-fold sample symmetry.

In the grain growth stage of oxidation on the sample RD, the effective 'base area' is the factor controlling the oxidation processes mainly because the stress at the metal/oxide interface is large. This stress can be reduced if, among all oxide nuclei shown in Fig. 4, the nuclei with the smallest effective 'base area' grow faster than other nuclei. Since the effective 'base area' is calculated from the (*hkl*) component of an oxide orientation, the most favorable crystallographic planes can be predicted in the stage of oxide growth. Table II lists crystallographic planes with a small effective 'base area' from the orientation shown in Fig. 4. One can see from this table, that the crystallographic planes ranging from

TABLE II Favorable oxide crystallographic planes in grain growth stage

Crystallographic planes parallel to the sample surface	*Base area* ($Å^2$)	*Effective base area*
(001)	27.04	22.71
(10$\bar{6}$)	26.67	22.28
(10$\bar{5}$)	26.73	22.26
(10$\bar{4}$)	26.83	22.24
(10$\bar{3}$)	27.14	22.41
(100)	27.93	23.46
(60$\bar{1}$)	27.50	22.94
(50$\bar{1}$)	27.58	22.97
(40$\bar{1}$)	27.66	22.99
(610)	28.30	23.77
(010)	27.25	22.89
(061)	27.61	23.19
(160)	27.63	23.21

(10$\bar{6}$) to (10$\bar{3}$) have a small effective 'base area' and are favorable among which the one with the (10$\bar{4}$) plane is the ideal oxide orientation. In other words, the oxide nuclei with the (10$\bar{4}$) crystallographic plane parallel to the sample surface will grow fastest. As a result, the (10$\bar{4}$)[010], (10$\bar{4}$)[401] and their equivalent orientations will become the ideal orientations of the oxide.

Certainly, the substrate of sample RD contains many other orientations except the ideal orientation listed in Table I. Given the proposed computer model, the ODF of the substrate can he introduced into the computer specimen and so that the oxide texture formation on sample RD, with all the substrate orientations, can be simulated. The simulated ODF is plotted in Fig. 5(a) and the ODF calculated experimental pole figures is plotted in Fig. 5(b) for comparison. Good agreement between the orientations predicted by the model and from the experimental data is clearly demonstrated in Fig. 5.

The orientation analyses for the oxides formed on samples TD and LD are the same as those described for the oxide formed on sample RD. The simulation shows that the orientations of oxide formed on the samples TD and LD, at the nucleation stage are $\{0nm\}\langle 100\rangle$. In this orientation group, the oxide orientations with a (10$\bar{4}$) crystallographic plane parallel to the sample surface, are most favorable in the grain growth stage and the oxide grains with these orientations grow faster. Therefore, the orientation of (10$\bar{4}$)[010] and its equivalent orientations

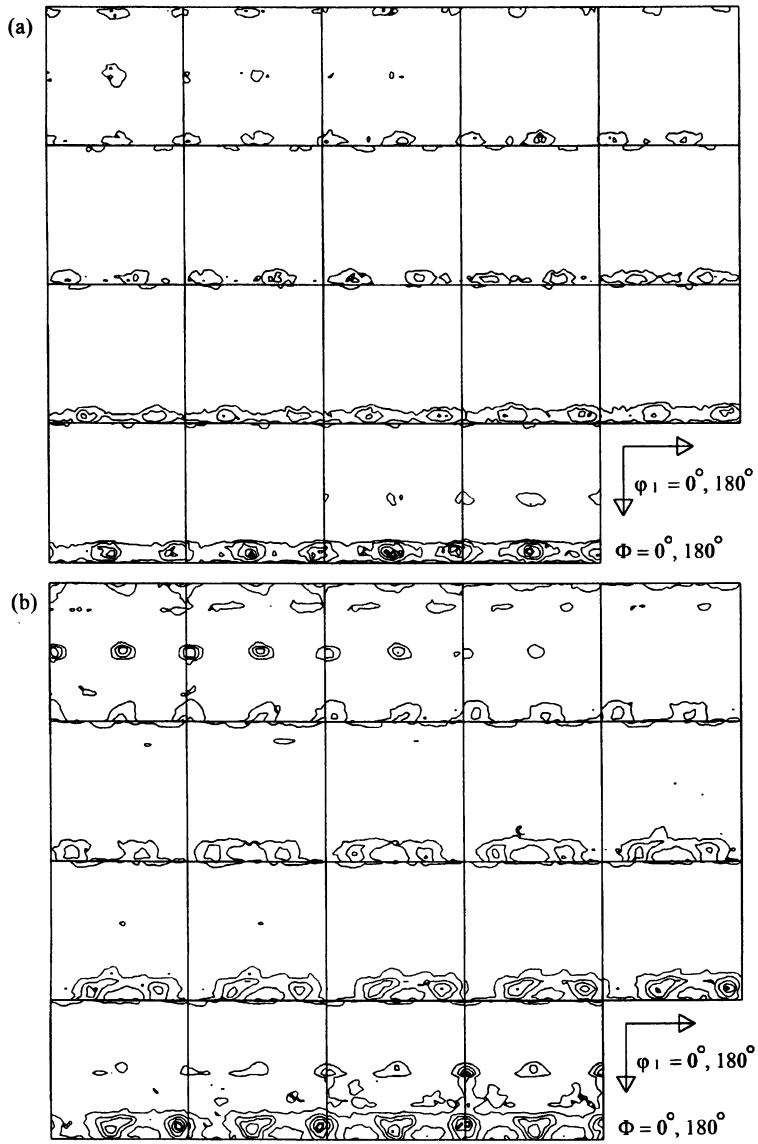

FIGURE 5 Comparison of the simulated and experimental ODFs of the oxide formed on sample RD. (a) Simulated ODF and (b) ODF calculated from experimental pole figures shown in the contour levels 3, 7, 11, 15, 19, 23.

should be stronger as the oxide grows and finally dominate all other orientations. Figure 6 shows the (111), (11$\bar{1}$) and (002) poles figures calculated from the simulated oxide ODF for the three samples, and Fig. 7 shows the experimental pole figures for the three samples. A good agreement between simulation results and the experimental data is also clearly seen in these figures.

Because of the brevity of this paper, not all the simulation results are presented. In brief, the simulation predicts the following major features of the oxide texture formed on the three samples: the major and minor oxide orientations, the orientation symmetry and the orientation spread. Part of these results can be found in Li *et al.* (1999).

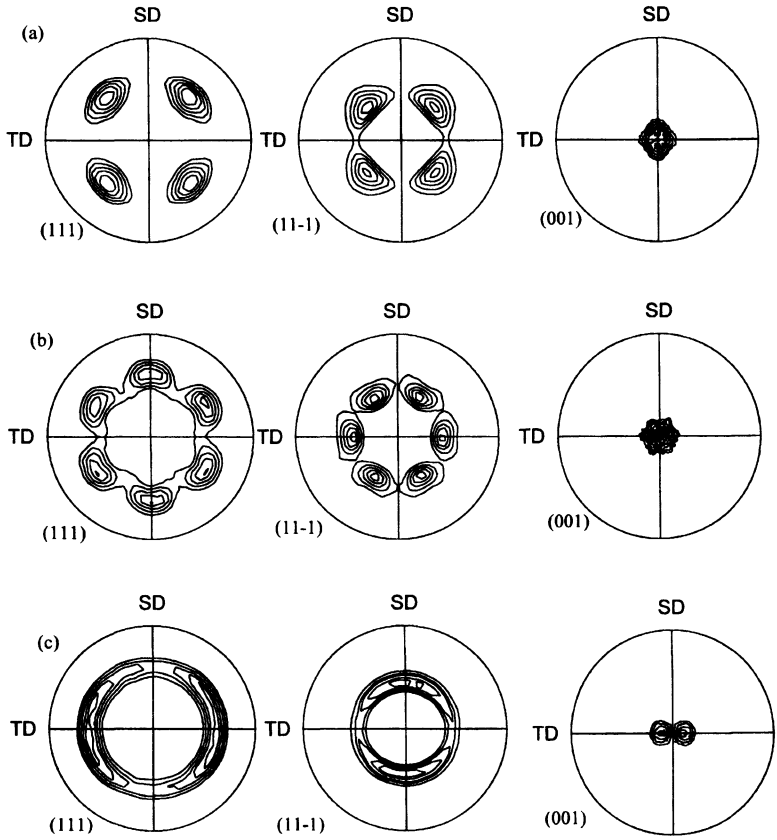

FIGURE 6 The pole figures calculated from the simulated ODFs of the oxide formed on (a) sample RD, (b) sample TD and (c) sample LD.

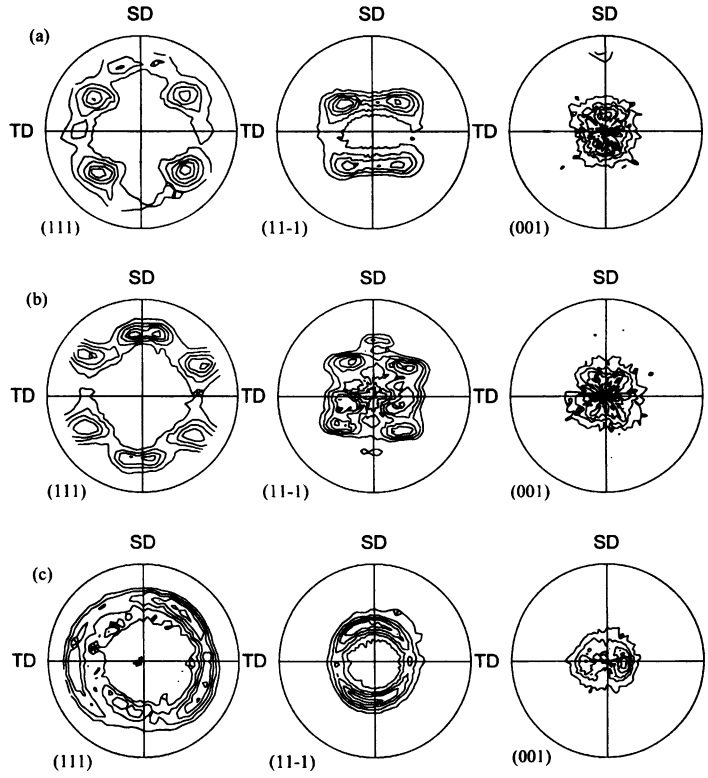

FIGURE 7 The experimental pole figures of the oxide formed on (a) sample RD, (b) sample TD and (c) sample LD.

CONCLUSIONS

A two-dimensional computer model is developed which is capable of simulating the texture and microstructure formation in ZrO_2 film. The model has been verified by the simulation of oxidation on three different substrate orientations and comparing them with experimental results. Good agreement has been obtained.

References

Beie, H.-J., Mitwalsky, A., Garzarilli, F., Ruhmann, H. and Sell, H.-J. (1994). *Zirconium in the Nuclear Industry: Tenth International Symposium*, ASTM STP 1245,

A.M. Garde and E.R. Bradley, Eds., p. 615, American Society for Testing and Materials, Philadelphia, PA.
Bunge, H.-J. (1982). *Texture Analysis in Materials Science*, Butterworth, UK.
Kofstad, P. (1988). *High-Temperature Corrosion*, Elsevier, New York, NY.
Li, H., Glavicic, M. and Szpunar, J.A. (1999). *Acta Meter.* (to be published).
Lin, Y.P., Woo, O.T. and Lockwood, D.J. (1994). Polycrystalline thin films: structure, properties and applications, *MRS Symp. Proc.*, USA, Vol. 343, 487 pp.
Ploc, R.A. (1983). *J. Nucl. Mater.*, **113**, 75.